Acta Oceanol. Sin., 2020, Vol. 39, No. 7, P. 115–126
https://doi.org/10.1007/s13131-020-1622-0
http://www.hyxb.org.cn
E-mail: hyxbe@263.net

Iterative analytical solution for wave reflection by a multi-chamber partially perforated caisson breakwater

Yang Zhao[1], Yong Liu[1]*, Huajun Li[1]

[1] Institute of Coastal and Ocean Engineering, Ocean University of China, Qingdao 266100, China

Received 28 May 2019; accepted 8 August 2019

Abstract

This study examines wave reflection by a multi-chamber partially perforated caisson breakwater based on potential theory. A quadratic pressure drop boundary condition at perforated walls is adopted, which can well consider the effect of wave height on the wave dissipation by perforated walls. The matched eigenfunction expansions with iterative calculations are applied to develop an analytical solution for the present problem. The convergences of both the iterative calculations and the series solution itself are confirmed to be satisfactory. The calculation results of the present analytical solution are in excellent agreement with the numerical results of a multi-domain boundary element solution. Also, the predictions by the present solution are in reasonable agreement with experimental data in literature. Major factors that affect the reflection coefficient of the perforated caisson breakwater are examined by calculation examples. The analysis results show that the multi-chamber perforated caisson breakwater has a better wave energy dissipation function (lower reflection coefficient) than the single-chamber type over a broad range of wave frequency and may perform better if the perforated walls have larger porosities. When the porosities of the perforated walls decrease along the incident wave direction, the perforated caisson breakwater can achieve a lower reflection coefficient. The present analytical solution is simple and reliable, and it can be used as an efficient tool for analyzing the hydrodynamic performance of perforated breakwaters in preliminary engineering design.

Key words: partially perforated caisson, multi-chamber, reflection coefficient, quadratic pressure drop, matched eigenfunction expansions, iterative calculation

Citation: Zhao Yang, Liu Yong, Li Huajun. 2020. Iterative analytical solution for wave reflection by a multi-chamber partially perforated caisson breakwater. Acta Oceanologica Sinica, 39(7): 115–126, doi: 10.1007/s13131-020-1622-0

1 Introduction

A perforated caisson breakwater with a wave absorbing chamber (Jarlan, 1961) has been often used to dissipate wave energy and reduce the reflection coefficient and wave force of the structure. In order to dissipate more wave energy, multi-chamber perforated caisson breakwaters have been applied in practical engineering (Franco, 1994; Franco et al., 1998; Bergmann and Oumeraci, 2000; Liu et al., 2012). In addition, a partially perforated caisson breakwater (the water depth inside the wave chamber is reduced) with better stability against sliding and overturning has been used instead of a fully perforated caisson breakwater (Liu et al., 2008a, 2009; Huang et al., 2011). To enhance both the wave energy dissipation performance and the structure stability, multi-chamber partially perforated caissons can be used for building breakwaters. The objective of this study is to develop a new analytical solution for wave reflection by multi-chamber partially perforated caisson breakwaters.

Many studies on wave interaction with perforated caisson breakwaters have been conducted. Experimental tests (Suh et al., 2001; Liu et al., 2008a) and numerical simulations (Chen et al., 2003; Ren and Ma, 2015; Aristodemo et al., 2015) have been conducted to clarify the wave energy dissipation mechanism of single-chamber perforated caisson breakwaters. Experimental tests have also been conducted to examine the hydraulic characteristics of multi-chamber perforated caisson breakwaters (Kondo, 1979; Kakuno and Nakata, 1998; Kakuno et al., 1999; Bergmann and Oumeraci, 2000; Chen et al., 2002; Lee et al., 2014). In addition to experimental and numerical studies, analytical solutions based on linear potential theory, which are very simple and efficient in computations, have been developed for estimating the reflection coefficients of perforated caissons. It is well known that wave energy dissipation by perforated walls cannot be considered in classical potential theory. Thus, suitable pressure drop (energy loss) boundary conditions on the perforated walls must be incorporated into the analytical solutions. Based on the porous medium model of Sollitt and Cross (1972), Yu (1995) developed a linear pressure drop condition to describe the relation between the pressure difference and the fluid velocity across the perforated wall. This boundary condition has been often used for developing analytical solutions to wave scattering by perforated structures (e.g., Isaacson et al., 1999; Li et al., 2003, 2005; Liu et al., 2008b; Koraim et al., 2011; Liu et al., 2012). Especially, Li et al. (2003) analytically examined oblique wave reflection by a perforated breakwater with two wave chambers; Liu et al. (2012) developed an analytical solution for oblique wave interaction with an infinite array of uniform multi-chamber fully perforated caissons.

Different from linear pressure drop condition, Mei et al. (1974) developed a quadratic pressure drop condition on the perforated wall in terms of jet through the holes under the long wave

Foundation item: The National Natural Science Foundation of China under contract Nos 51725903 and 51490675.
*Corresponding author, E-mail: liuyong@ouc.edu.cn

assumption. This nonlinear pressure drop condition was further extended to general wave conditions by Bennett et al. (1992). Molin and Fourest (1992) also developed a different quadratic pressure drop condition on perforated wall and then studied the performance of a multi-chamber perforated wave absorber in the wave flume. The beauty of quadratic pressure drop conditions is that the influence of wave height on the wave energy dissipation can be directly incorporated into the mathematical models. However, iterative calculations are needed to solve the nonlinear boundary condition. A linearized version of the quadratic pressure drop condition was used by Suh et al. (2006) for analyzing wave reflection by a single-chamber partially perforated caisson on a rubble mound foundation. Recently, based on the quadratic pressure drop condition, Liu and Li (2017) developed a multi-domain BEM (Boundary element method) solution for wave reflection by a single-chamber partially perforated caisson breakwater, and iterative calculations were conducted in their solution.

To the best knowledge of authors, a fully analytical solution for wave reflection by multi-chamber partially perforated caisson breakwaters involving quadratic pressure drop condition has not been developed so far. This is just the objective of this study. For preliminary engineering design, such an analytical solution is valuable for fast accessing the hydrodynamic performance of multi-chamber perforated caisson breakwaters under different conditions. Moreover, a better understanding in wave reflection by perforated wall structures can be obtained during the analytically solving procedure. In the following Section, the analytical model of the present problem is developed using matched eigenfunction expansions with iterative calculations. In Section 3, the convergences of the iterative procedure and the series solution itself are both examined. The present iterative analytical solution is also compared with a multi-domain BEM solution. Moreover, the analytical solution is verified using experimental data in literature. In Section 4, calculation examples are presented to examine the effects of major factors on the reflection coefficient of breakwater, and valuable results are given as reference for engineering design. Finally, the main conclusions of this study are drawn.

2 Analytical solution

The ideal sketch of the present problem is illustrated in Fig. 1. The partially perforated caisson breakwater has N wave chambers, and the widths of the chambers along the wave incident direction are S_1, S_2, ... and S_N, respectively. The total width of all the chambers is S. The breakwater is set in the ocean of constant depth h, and the water depth in the wave chamber is d. If $d = h$, this structure becomes a fully perforated caisson breakwater. A Cartesian coordinate system, with the origin at the still water level and the z-axis pointing upwards along the first perforated wall, is used for the mathematical description. The whole fluid domain is divided into (N+1) regions: region 0, the fluid domain in front of the breakwater; region N, the fluid domain occupied by the N-th wave chamber. The j-th perforated wall is located at $x = l_j$ ($l_1 = 0$), and the rear solid wall is located at $x = l_{N+1} = S$. When considering wave reflection by the whole breakwater, the thickness of each perforated wall is assumed to be zero as it is very small compared to the incident wavelength L.

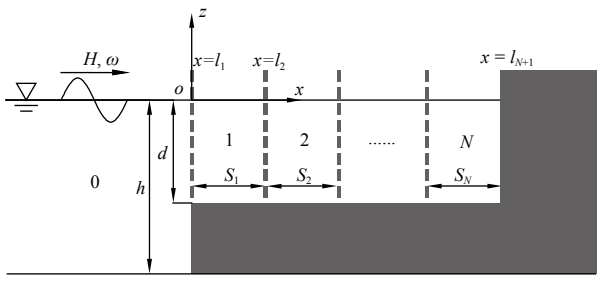

Fig. 1. Idealized sketch for wave reflection by a multi-chamber partially perforated caisson breakwater.

Based on the potential theory, it is assumed that the fluid is inviscid and incompressible, and its motion is irrotational. For time-harmonic incident wave with angular frequency ω, the time factor $e^{-i\omega t}$ can be separated, and the velocity potential Φ in each region can be written as

$$\Phi_j(x,z,t) = \mathrm{Re}\left\{\phi_j(x,z)\,e^{-i\omega t}\right\},\ j = 0,1,2,...,N, \tag{1}$$

where Re denotes the real part of variables, and ϕ_j is the complex spatial velocity potential in region j.

The spatial velocity potential in each region satisfies the Laplace equation:

$$\frac{\partial^2\phi_j}{\partial x^2} + \frac{\partial^2\phi_j}{\partial z^2} = 0,\ j = 0,1,2,...,N. \tag{2}$$

The complex potentials satisfy the linearized free surface boundary condition:

$$\frac{\partial\phi_j(x,z)}{\partial z} = \frac{\omega^2}{g}\phi_j(x,z),\ z = 0,\ j = 0,1,2,...,N, \tag{3}$$

where g means the gravitational acceleration. On the seabed and the bottom of wave chambers, the complex potentials satisfy the impermeable boundary condition:

$$\frac{\partial\phi_0(x,z)}{\partial z} = 0,\ z = -h,\ x \leqslant 0, \tag{4}$$

$$\frac{\partial\phi_j(x,z)}{\partial z} = 0,\ z = -d,\ l_j < x < l_{j+1}, j = 1,2,...,N. \tag{5}$$

On the left far field, the reflected waves must be outgoing:

$$\lim_{x\to-\infty}\left(\frac{\partial}{\partial x} + ik_0\right)(\phi_0 - \phi_I) = 0, \tag{6}$$

where ϕ_I is the velocity potential of incident waves, k_0 denotes the wave number of incident wave in water depth h.

When the fluid passes through the perforated walls, the averaged horizontal fluid velocity is continuous:

$$\frac{\partial\phi_0(x,z)}{\partial x} = \begin{cases} \dfrac{\partial\phi_1(x,z)}{\partial x}, & -d \leqslant z \leqslant 0 \\ 0, & -h \leqslant z < -d \end{cases},\ x = 0, \tag{7}$$

$$\frac{\partial\phi_{j-1}(x,z)}{\partial x} = \frac{\partial\phi_j(x,z)}{\partial x},\ -d \leqslant z \leqslant 0,\ x = l_j,\ j = 2,3,...,N. \tag{8}$$

In addition, a part of wave energy is dissipated by the perforated walls, and the phase of fluid motion may be slightly changed due to the inertial effect of perforated walls. Here, we use a quad-

ratic pressure drop condition to represent both the energy loss and the phase shift. At the j-th perforated wall, the quadratic pressure drop condition is written as (Molin and Fourest, 1992; Molin and Remy, 2015; Liu and Li, 2017):

$$\phi_{j-1}-\phi_j=-\frac{8\mathrm{i}}{3\pi\omega}\frac{1-\varepsilon_j}{2\mu_j\varepsilon_j^2}\left|\frac{\partial\phi_j}{\partial x}\right|\frac{\partial\phi_j}{\partial x}-2C_j\frac{\partial\phi_j}{\partial x},\quad -d\leqslant z\leqslant 0,\ x=l_j,\ j=1,2,...,N, \tag{9}$$

where μ is the discharge coefficient of perforated wall, ε is the geometrical porosity of perforated wall, C is the blockage coefficient of perforated wall, and the subscript j denotes the parameters of the j-th perforated wall. The first and second terms on the right-hand side of Eq. (9) denote the resistance effect (energy loss) and inertial effect (phase shift) of the perforated wall, respectively. If the resistance term is equal to 0, there will be no energy loss around the perforated wall.

For practical calculations, the discharge coefficient μ and the blockage coefficient C should be known a prior. Molin et al. (2011) recommended the value of μ = 0.3 – 0.4 at ε < 0.5. Using the values of μ = 0.4 and 0.7 for the fully and partially perforated caissons, respectively, Liu and Li (2017) have achieved a good agreement between the multi-domain BEM solution and the experimental data. In this study, the values of μ = 0.4 and 0.7 are also adopted for the fully and partially perforated caissons, respectively. The blockage coefficient for a slotted wall can be estimated using the following formula (Taylor, 1973; Kakuno and Liu, 1993):

$$C=\frac{a}{2}\left(\frac{1}{\varepsilon}-1\right)+\frac{b}{\pi}\left[1-\ln(4\varepsilon)+\frac{1}{3}\varepsilon^2+\frac{281}{180}\varepsilon^4\right], \tag{10}$$

where a is the wall thickness and b is the spacing between the centers of two adjacent slats, as shown in Fig. 2. It is noted that the wall thickness is only considered in estimating the blockage coefficient. In the following calculations, the blockage coefficient is determined by Eq. (10) unless otherwise noted.

On the rear solid wall of the perforated caisson, the non-penetration boundary condition is:

$$\frac{\partial\phi_N}{\partial x}=0,\ x=l_{N+1}. \tag{11}$$

Now, we use the matched eigenfunction expansion method to determine the velocity potentials in all regions. The velocity potentials, which satisfy the Laplace equation (2) and the relevant boundary conditions in (3)–(6), can be written as:

$$\phi_0=\frac{-\mathrm{i}gH}{2\omega}\left[\mathrm{e}^{\mathrm{i}k_0x}Z_0(z)+R_0\mathrm{e}^{-\mathrm{i}k_0x}Z_0(z)+\sum_{n=1}^{\infty}R_n\mathrm{e}^{k_nx}Z_n(z)\right], \tag{12}$$

$$\phi_j=\frac{-\mathrm{i}gH}{2\omega}\left[\begin{array}{l}A_{j,0}\cos\lambda_0\left(x-\dfrac{l_j+l_{j+1}}{2}\right)Y_0(z)+\\ \displaystyle\sum_{n=1}^{\infty}A_{j,n}\frac{\cosh\lambda_n\left(x-\frac{l_j+l_{j+1}}{2}\right)}{\cosh\lambda_n\left(\frac{l_{j+1}-l_j}{2}\right)}Y_n(z)+\\ B_{j,0}\sin\lambda_0\left(x-\dfrac{l_j+l_{j+1}}{2}\right)Y_0(z)+\\ \displaystyle\sum_{n=1}^{\infty}B_{j,n}\frac{\sinh\lambda_n\left(x-\frac{l_j+l_{j+1}}{2}\right)}{\cosh\lambda_n\left(\frac{l_{j+1}-l_j}{2}\right)}Y_n(z)\end{array}\right],j=1,2,...,N, \tag{13}$$

in which, H means the incident wave height; R_n, $A_{j,n}$ and $B_{j,n}$ (j = 1, 2,..., N; n = 0, 1,...) are unknown expansion coefficients to be determined; k_n, λ_n (n = 0, 1,...) are the positive real roots of the following dispersion relations:

$$\omega^2=gk_0\tanh(k_0h)=-gk_n\tan(k_nh),\ n=1,2,..., \tag{14}$$

$$\omega^2=g\lambda_0\tanh(\lambda_0d)=-g\lambda_n\tan(\lambda_nd),\ n=1,2,.... \tag{15}$$

$Z_n(z)$ and $Y_n(z)$ in Eqs (12) and (13) are vertical eigenfuctions as follows:

$$Z_0(z)=\frac{\cosh k_0(z+h)}{\cosh(k_0h)}, \tag{16}$$

$$Z_n(z)=\frac{\cos k_n(z+h)}{\cos(k_nh)},\ n=1,2,..., \tag{17}$$

$$Y_0(z)=\frac{\cosh\lambda_0(z+d)}{\cosh(\lambda_0d)}, \tag{18}$$

$$Y_n(z)=\frac{\cos\lambda_n(z+d)}{\cos(\lambda_nd)},n=1,2,.... \tag{19}$$

Based on the boundary conditions in Eqs (7)–(9) and (11), a system of equations with unknown expansion coefficients R_n, $A_{j,n}$ and $B_{j,n}$ can be obtained. For example, inserting Eqs (12) and (13) into Eq. (7), we have:

$$-\mathrm{i}k_0(R_0-1)+\sum_{n=1}^{\infty}R_nk_nZ_n(z)=\left[\begin{array}{l}A_{1,0}\lambda_0\sin\left(\lambda_0\dfrac{S_1}{2}\right)Y_0(z)+B_{1,0}\cos\left(\lambda_0\dfrac{S_1}{2}\right)\lambda_0Y_0(z)-\\ \displaystyle\sum_{n=1}^{\infty}A_{1,n}\lambda_n\tanh\left(\lambda_n\frac{S_1}{2}\right)Y_n(z)+\sum_{n=1}^{\infty}B_{1,n}\lambda_nY_n(z)\end{array}\right]. \tag{20}$$

Multiplying both sides of Eq. (20) by $Z_m(z)$ and integrating

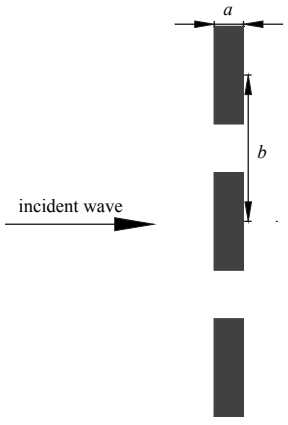

Fig. 2. Geometrical parameters for a perforated wall.

with respect to z along the whole water depth, we have:

$$\{R_m\} + [a_{mn}]\{A_{1,n}\} + [b_{mn}]\{B_{1,n}\} = \delta_m, \tag{21}$$

in which,

$$a_{mn} = -\frac{\lambda_0}{\kappa_m}\sin\left(\lambda_0\frac{S_1}{2}\right)\frac{\int_{-d}^{0} Y_0(z)Z_m(z)\,\mathrm{d}z}{\int_{-h}^{0} Z_m^2(z)\,\mathrm{d}z},\ n=0, \tag{22}$$

$$a_{mn} = \frac{\lambda_n}{\kappa_m}\tanh\left(\lambda_n\frac{S_1}{2}\right)\frac{\int_{-d}^{0} Y_n(z)Z_m(z)\,\mathrm{d}z}{\int_{-h}^{0} Z_m^2(z)\,\mathrm{d}z},\ n\neq 0, \tag{23}$$

$$b_{mn} = -\frac{\lambda_0}{\kappa_m}\cos\left(\lambda_0\frac{S_1}{2}\right)\frac{\int_{-d}^{0} Y_0(z)Z_m(z)\,\mathrm{d}z}{\int_{-h}^{0} Z_m^2(z)\,\mathrm{d}z},\ n=0, \tag{24}$$

$$b_{mn} = -\frac{\lambda_n}{\kappa_m}\frac{\int_{-d}^{0} Y_n(z)Z_m(z)\,\mathrm{d}z}{\int_{-h}^{0} Z_m^2(z)\,\mathrm{d}z},\ n\neq 0, \tag{25}$$

$$\delta_m = 1,\ m=0, \tag{26}$$

$$\delta_m = 0,\ m\neq 0, \tag{27}$$

$$\kappa_m = -\mathrm{i}k_0, m=0, \tag{28}$$

$$\kappa_m = k_m,\ m\neq 0. \tag{29}$$

Employing the similar methods as above, we can obtain another four sets of equations:

$$[c_{j,mn}]\{A_{j,n}\} + [d_{j,mn}]\{B_{j,n}\} + [e_{j,mn}]\{A_{j+1,n}\} + [f_{j,mn}]\{B_{j+1,n}\} = 0, \tag{30}$$

$$[g_{mn}]\{R_n\} + [h_{mn}]\{A_{1,n}\} + [t_{mn}]\{B_{1,n}\} = \sigma_m, \tag{31}$$

$$[p_{j,mn}]\{A_{j,n}\} + [q_{j,mn}]\{B_{j,n}\} + [r_{j,mn}]\{A_{j+1,n}\} + [s_{j,mn}]\{B_{j+1,n}\} = 0, \tag{32}$$

$$[u_{mn}]\{A_{N,n}\} + [v_{mn}]\{B_{N,n}\} = 0, \tag{33}$$

where $j=1, 2, \ldots, N-1$. The matrix coefficients in Eqs (30)–(33) are listed in Appendix.

By truncating m and n after M terms in Eqs (21) and (30) – (33), the above five sets of equations can be solved. It is noted that the carefully selected expressions of trigonometric and hyperbolic tangent functions in Eq. (13) are helpful to get convergent results in the above solving procedure (Zhao et al., 2017). It is also noted that Eqs (31) and (32) include nonlinear terms due to the quadratic pressure drop condition in Eq. (9). Thus, iterative calculations must be employed to solve the nonlinear system of equations. The specific iterative calculation procedure is given as follows.

(1) Setting the initial guesses, $A_{j,n}^{(1)}$ and $B_{j,n}^{(1)}$, to be zero, then the value of $\Psi_j(z)$ in Eq. (A8) is determined and the equations become a linear system.

(2) Assuming that the iterative procedure reaches the K-th step, and $A_{j,n}^{(K)}$ and $B_{j,n}^{(K)}$ are the K-th approximation, then the updated (K+1)-th approximations of $A_{j,n}^{(K+1)}$ and $B_{j,n}^{(K+1)}$ are obtained by solving the linear system using Gauss elimination method.

(3) Evaluating the differences of all the coefficients between the K-th approximation and the (K+1)-th approximation; if the absolute value of each difference is larger than the required precision (10^{-4} is used in this study), setting the averaged values of them to be the new initial values and repeating step 2; otherwise, stopping the iterative calculation and required results are determined.

3 Validations

3.1 *Convergence examinations*

The convergences of both the iterative procedure and the series solution itself are significant for giving accurate and reliable results, and thus they are firstly examined.

The iterative calculation results of typical unknown expansion coefficients of R_0, $A_{1,0}$, $B_{2,0}$ and $A_{3,1}$ in each step are shown in Table 1. In the calculations, the truncated number of $M=12$ is used and the other calculation conditions are: $N=3$, $H/h=0.15$, $k_0h=1.5$, $d/h=0.5$, $S/h=0.9$, $S_j=S/N$, $\varepsilon_j=0.25$, $a_j/h=0.02$ and $b_j/h=0.08$ ($j=1, 2, 3$). It can be seen from Table 1 that the iterative calculations have a good convergence, and the required accuracy (10^{-4}) are reached after 14 steps. In fact, for almost all the iterative calculations in this study, the convergent results are obtained after no more than 20 iterative steps.

The typical calculation results of the reflection coefficient C_R at different truncated number M are listed in Table 2. The calculating conditions are: $N=3$, $H/h=0.15$, $d/h=0.5$, $S/h=0.9$, $S_j=S/N$, $\varepsilon_j=0.25$, $a_j/h=0.02$ and $b_j/h=0.08$ ($j=1, 2, 3$). It can be seen from Table 2 that the convergence of the present series solution is fast. Using the value of $M=10$ can ensure the accuracy to third decimal places, which is enough for engineering purposes. Thus, the value of $M=10$ is adopted in the following calculations. It can be seen from above analysis that the present iterative analytical model has very good calculation efficiency.

3.2 *Comparison with multi-domain BEM solution*

For cross-checking, we have also solved the present problem using the iterative multi-domain BEM (Liu and Li, 2017). Compared with the analytical solution, the multi-domain BEM solution is a more cumbersome numerical solution and all the fluid boundaries need to be discretized. In the multi-domain BEM solution, a vertical fictional boundary with a distance l away from the perforated caisson breakwater was introduced. A large value of $l=3h$ was used for avoiding the effect of evanescent modes of the velocity potential in the outer flow field. According to our numerical examinations, each boundary element size was set to be $h/50$ and then convergent numerical results were obtained.

The reflection coefficients C_R calculated by the present analytical solution and the multi-domain BEM solution are compared in Fig. 3. Both fully and partially perforated caisson break-

Table 1. Convergence examination of the iterative calculations

Iterative step	Expansion coefficient			
	R_0	$A_{1,0}$	$B_{2,0}$	$A_{3,1}$
0	–	0.0	0.0	0.0
1	–0.188 55 + 0.982 06i	0.087 39 + 0.105 77i	–0.930 03 – 1.125 57i	–0.000 16 – 0.000 19i
2	0.340 07 + 0.032 88i	0.579 30 – 0.381 55i	–0.325 02 – 0.389 64i	–0.006 93 + 0.000 37i
6	0.303 64 + 0.081 74i	0.540 17 – 0.319 52i	–0.349 98 – 0.456 64i	–0.005 16 + 0.000 55i
7	0.304 14 + 0.082 25i	0.538 79 – 0.318 08i	–0.349 74 – 0.456 95i	–0.005 15 + 0.000 55i
8	0.304 34 + 0.082 49i	0.538 16 – 0.317 42i	–0.349 65 – 0.457 12i	–0.005 15 + 0.000 55i
12	0.304 47 + 0.082 69i	0.537 69 – 0.316 91i	–0.349 59 – 0.457 28i	–0.005 15 + 0.000 55i
13	0.304 48 + 0.082 69i	0.537 68 – 0.316 90i	–0.349 59 – 0.457 28i	–0.005 15 + 0.000 55i
14	0.304 48 + 0.082 69i	0.537 67 – 0.316 89i	–0.349 59 – 0.457 28i	–0.005 15 + 0.000 55i

Note: "–" is ***.

Table 2. Convergence of C_R with the increasing truncated number M

Truncated number	Reflection coefficient (C_R)						
	S/L = 0.01	S/L = 0.05	S/L = 0.10	S/L = 0.20	S/L = 0.40	S/L = 0.60	S/L = 0.80
2	0.997 1	0.752 1	0.402 0	0.304 5	0.337 2	0.261 7	0.389 7
5	0.997 1	0.751 7	0.400 6	0.304 7	0.336 6	0.262 1	0.388 2
8	0.997 1	0.751 6	0.400 3	0.304 7	0.336 2	0.262 0	0.388 5
10	0.997 1	0.751 6	0.400 2	0.304 7	0.336 1	0.261 9	0.388 5
12	0.997 1	0.751 6	0.400 2	0.304 7	0.336 1	0.261 9	0.388 5
40	0.997 1	0.751 6	0.400 2	0.304 7	0.336 0	0.261 9	0.388 5

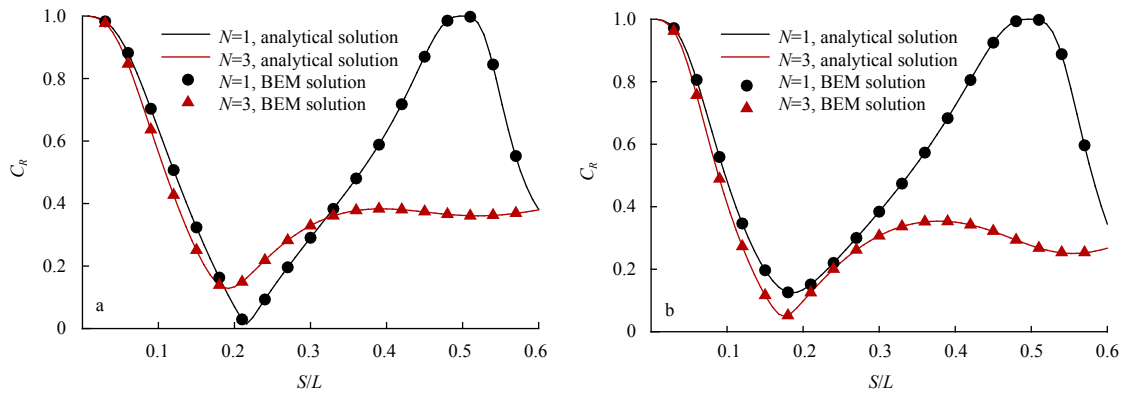

Fig. 3. Comparison between the present analytical solution and the multi-domain BEM solution. a. Fully perforated caisson breakwater and b. partially perforated caisson breakwater.

waters with one or three chambers (N = 1 and 3) are examined. The calculation conditions of H/h = 0.2, S/h = 0.6, $S_j = S/N$, ε_j = 0.33, a_j/h = 0.02 and b_j/h = 0.09 are adopted for all the caissons in Fig. 3. The relative water depths inside the chamber are d/h = 1.0 in Fig. 3a and d/h = 0.6 in Fig. 3b. The lines and dots in Fig. 3 denote the analytical solution and the multi-domain BEM solution, respectively. It is evident that the agreement between two different solutions is excellent.

3.3 *Comparison with experimental data*

Kondo (1979) and Kakuno et al. (1999) have experimentally measured the reflection coefficients of two-chamber fully and partially perforated caisson breakwaters, respectively. Figures 4 and 5 give the comparisons between the present calculation results and the experimental data of Kondo (1979) and Kakuno et al. (1999), respectively.

The calculation conditions in Fig. 4 for the two-chamber fully perforated caisson breakwater are: H = 0.04 m, $h = d$ = 1 m, $S_1 = S_2$ = 0.25 m, ε_2 = 0.2, $a_1 = a_2$ = 0.006 m. The porosity of the first perforated wall is ε_1 = 0.34 in Fig. 4a and ε_1 = 0.20 in Fig. 4b. In the present calculations, the blockage coefficient of perforated wall is determined by the empirical formula $C = a/2\varepsilon$ (Suh et al., 2011; Huang et al., 2011), as the holes of the perforated wall are circular shape. It can be seen from Fig. 4 that the overall agreement between the calculation results and the experimental data is reasonable. But, the present calculation results are smaller than the experimental results for large S/L in Fig. 4a. One possible reason is that the value of the discharge coefficient μ used here may be not most suitable for practical application, as the discharge coefficient μ may be relevant to the wave parameters and structure factors.

For the two-chamber partially perforated caisson breakwater in Fig. 5, the chamber widths are: S_1 = 0.125 m and S_2 = 0.198 m in Fig. 5a; S_1 = 0.109 m and S_2 = 0.183 m in Fig. 5b. Two different wave steepness of H/L = 0.01 and 0.03 are considered in Fig. 5. The other calculation conditions are: h = 0.5 m, d = 0.15 m, ε_1 = 0.4, ε_2 = 0.2, a_1 = 0.02 m, a_2 = 0.017 m, b_1 = 0.05 m and b_2 = 0.044 m. It can be seen from Fig. 5 that for two different wave steepness,

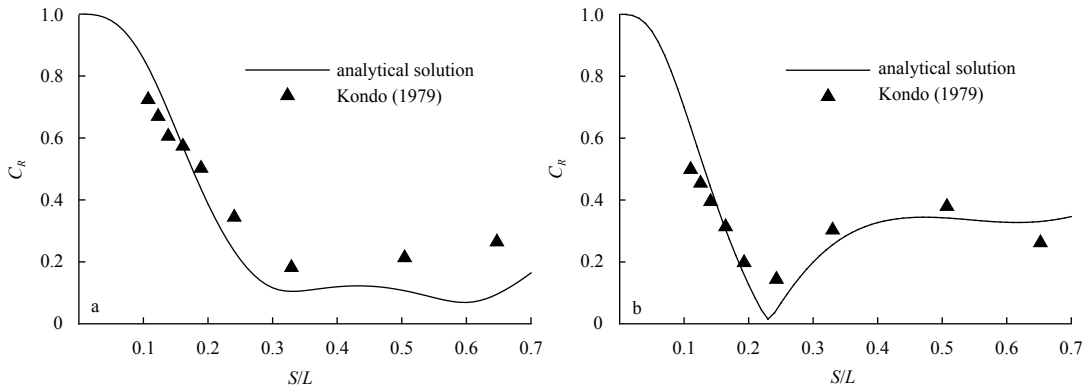

Fig. 4. Comparison between the present analytical solution and the experimental data of Kondo (1979) for a two-chamber fully perforated caisson breakwater. a. $\varepsilon_1 = 0.34$ and b. $\varepsilon_1 = 0.20$.

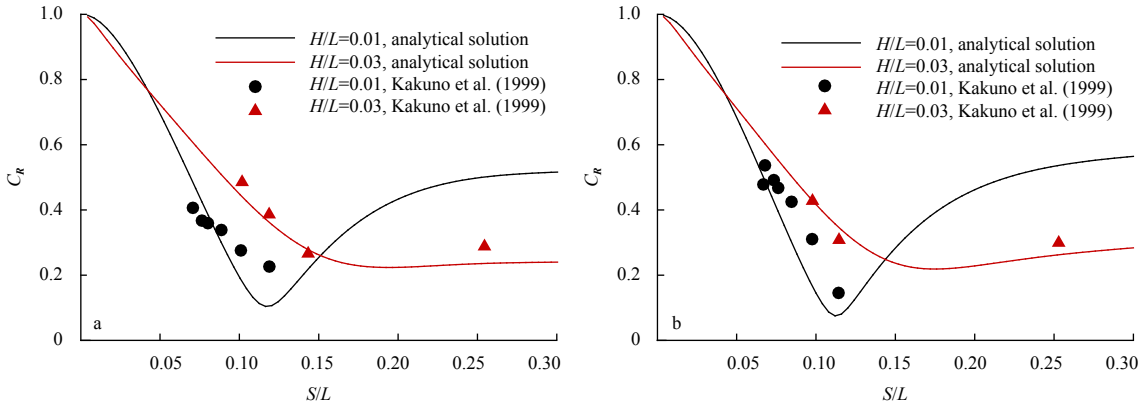

Fig. 5. Comparison between the present analytical solution and the experimental results of Kakuno et al. (1999) for a two-chamber partially perforated caisson breakwater. a. $S_1 = 0.125$ m and $S_2 = 0.198$ m and b. $S_1 = 0.109$ m and $S_2 = 0.183$ m.

the agreements between the present calculation results and the experimental data of Kakuno et al. (1999) are both good. This means that the effect of wave height on the reflection coefficient (wave energy dissipation) can be well considered in the present analytical solution.

4 Calculation examples with discussion

The influences of the wave chamber number N, the relative water depth in the chamber d/h, the dimensionless chamber width S_j/h and the porosity of each perforated wall ε_j ($j = 1, 2, \ldots, N$) on the reflection coefficient are examined by calculation examples. In practical engineering, the common porosity of perforated caissons is about 0.2–0.4. Generally, the porosity of the perforated wall should be no larger than 0.4 due to the requirement of the structural strength. In the following calculations, the slat length is assumed to be constant and three different porosities of 0.25, 0.33 and 0.4 are considered. The corresponding values of b and a are listed in Table 3.

Figure 6 gives the effect of the wave chamber number N on the reflection coefficient C_R at a fixed total dimensionless chamber width of $S/h = 0.6$. The wall porosities ε_j ($j = 1, 2, 3, 4$) in Fig. 6a and Fig. 6b are 0.25 and 0.40, respectively. The other calculation conditions are: $H/h = 0.15$, $d/h = 0.50$ and $S_j = S/N$ ($j = 1, 2, \ldots, N$). It can be seen from Fig. 6 that for the single-chamber caisson breakwater ($N = 1$), the reflection coefficient reaches its minimum value at $S/L \approx 0.17$, in which the breakwater has the best wave dissipation performance. However, the reflection coefficient of the single-chamber caisson breakwater is about unity at $S/L \approx 0.15$ (no wave energy dissipation). Similar to the single-chamber caisson breakwater, the reflection coefficient of the multi-chamber caisson breakwater reaches its minimum value at $S/L \approx 0.17$, but with the further increasing value of S/L, the multi-chamber caisson breakwater can always keep low reflection. Then, the multi-chamber caisson breakwater has a better wave energy dissipation performance over a broad range of wave frequency compared with the single-chamber caisson breakwater. This is attractive for practical engineering in the sea with random waves. We can also see in Fig. 6 that the single-chamber breakwater with $\varepsilon_j = 0.25$ and four-chamber breakwater with $\varepsilon_j = 0.40$ both have good wave energy dissipation performance in the engineering interest condition of $0.1 < S/L < 0.3$. It is concluded that adding perforated walls is helpful in enhancing the breakwater's wave energy dissipation performance when the porosity of the front perforated wall is relatively large. This has also been found by Chen et al. (2002).

Table 3. The values of ε, b and a for perforated walls using in calculation examples

Parameters	Values		
ε	0.25	0.33	0.40
b/h	0.08	0.09	0.10
a/h	0.02	0.02	0.02

Figure 7 shows the effect of the wave chamber number N on

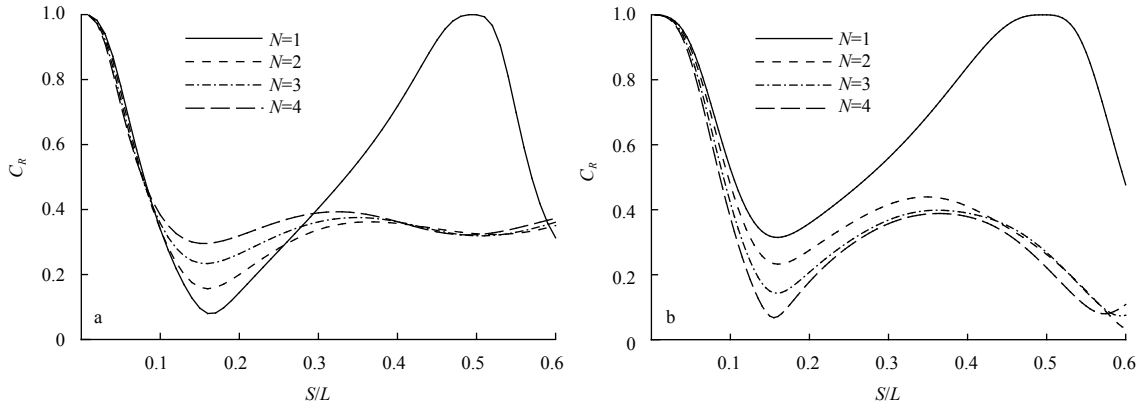

Fig. 6. Effect of the wave chamber number N on the reflection coefficient C_R at fixed S/h. a. $\varepsilon_j = 0.25$ ($j = 1, 2, 3, 4$), and b. $\varepsilon_j = 0.40$ ($j = 1, 2, 3, 4$).

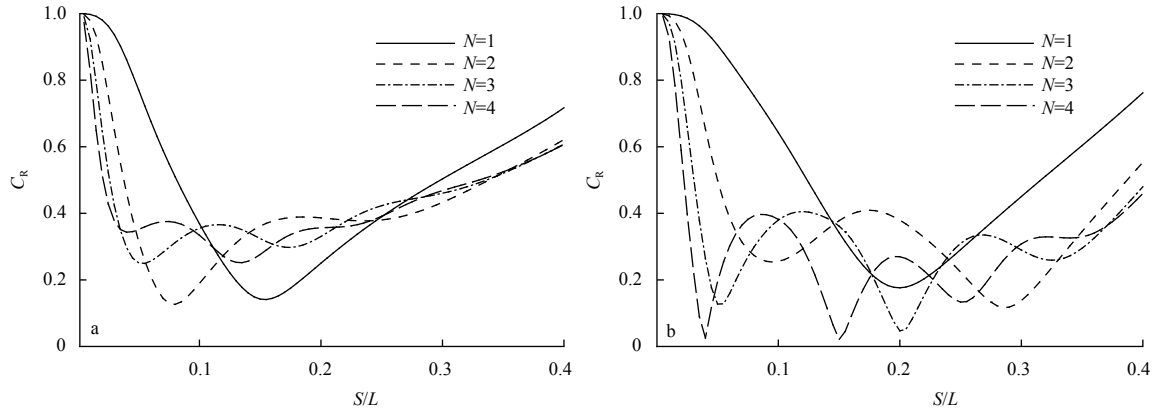

Fig. 7. Effect of the wave chamber number N on the reflection coefficient C_R at fixed S_j/h. a. $\varepsilon_j = 0.25$ ($j = 1, 2, 3, 4$) and b. $\varepsilon_j = 0.40$ ($j = 1, 2, 3, 4$).

the reflection coefficient C_R at fixed chamber width of $S_j/h = 0.225$. The calculation conditions are: $H/h = 0.15$, $d/h = 0.5$ and $S_j = S/N$. The wall porosities ε_j ($j = 1, 2, 3, 4$) in Fig. 7a and Fig. 7b are 0.25 and 0.40, respectively. For the case of $\varepsilon_j = 0.25$, the single-chamber caisson breakwater has a better wave energy dissipation performance in the range of $0.1 < S_j/L < 0.25$, while the multi-chamber type behaves much better when $S_j/L < 0.1$. For the case of $\varepsilon_j = 0.40$, the multi-chamber caisson breakwaters generally have a lower reflection coefficient than the single-chamber type. In a whole, the multi-chamber perforated caisson breakwater with higher porosity can dissipate more wave energy.

Figure 8 examines the effect of the porosity ε_j of each perforated wall on the reflection coefficient C_R. The wave chamber numbers are $N = 2$ in Fig. 8a and $N = 3$ in Fig. 8b. The other calculation conditions are: $H/h = 0.15$, $d/h = 0.5$ and $S_j = S/N = 0.3h$. The porosities of perforated walls are adopted as follows (along the incident wave propagation direction): uniform large porosity (40%), uniform small porosity (25%), gradually increasing porosities and gradually decreasing porosities. It can be seen from Fig. 8 that except for very long wave condition, the perforated caisson breakwater having perforated walls with gradually decreasing porosities usually can dissipate more incident wave energy and lead to a smaller reflection coefficient. Thus, the porosities of the perforated walls should decrease along the incident wave propagation direction in practice.

Different from porosities of multi-chamber perforated caisson breakwaters, uniform width of wave chambers is usually used in practical engineering. Here we present calculation results in Fig. 9 to see whether the wave energy dissipation performance of perforated caissons can be enhanced by using non-uniform wave chambers instead of uniform chambers. In Fig. 9, we consider three different combinations of the wave chamber widths (along the incident wave propagation direction): the gradually increasing case, the uniform case and the gradually decreasing case. The calculation conditions are: $H/h = 0.15$, $d/h = 0.5$, $\varepsilon_j = 0.25$ as well as $N = 2$ in Fig. 9a and $N = 3$ in Fig. 9b. In engineering interest range of $0.1 < S/L < 0.3$, using two wave chambers with increasing widths or three wave chambers with gradually decreasing widths instead of uniform chambers can decrease the reflection coefficient of the breakwater. The widths of non-uniform wave chambers in practical engineering should be carefully determined according to different chamber numbers.

Figure 10 examines the effect of the relative water depth in the wave chamber d/h on the reflection coefficient C_R. The wave chamber numbers are $N = 2$ and 3 in Figs 10a and 10b, respectively. The other calculation conditions are: $H/h = 0.15$, $S_j = S/N = 0.3h$, $\varepsilon_j = 0.25$ as well as $d/h = 0.25$, 0.5 and 0.75. It is evident from Fig. 10 that the effect of d/h on C_R is significant. In the range of $0.1 < S/L < 0.3$ for engineering interest, the wave dissipation performance for the caisson breakwater with $d/h = 0.5 - 0.75$ is much better than that for the breakwater with $d/h = 0.25$.

5 Concluding remarks

Based on the potential theory and the quadratic pressure

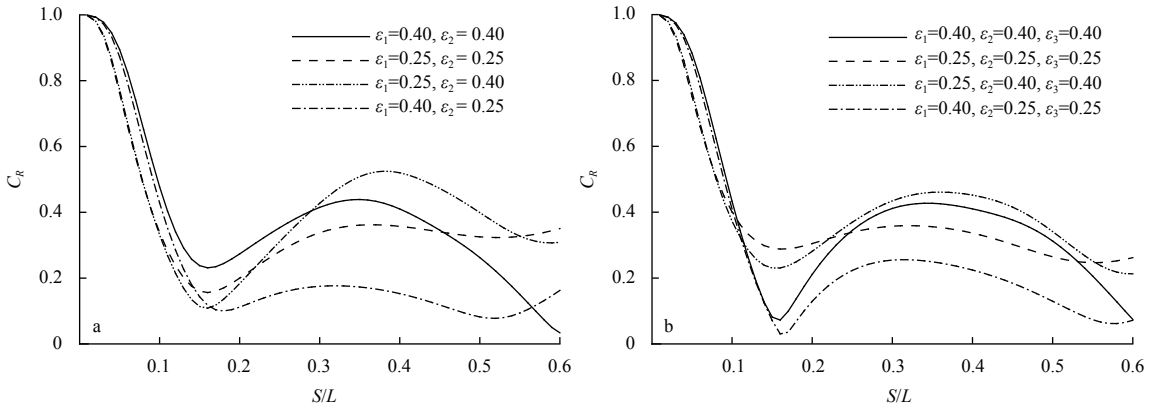

Fig. 8. Effect of the porosity ε_j of each perforated wall on the reflection coefficient C_R. a. Two-chamber perforated caisson breakwater and b. three-chamber perforated caisson breakwater.

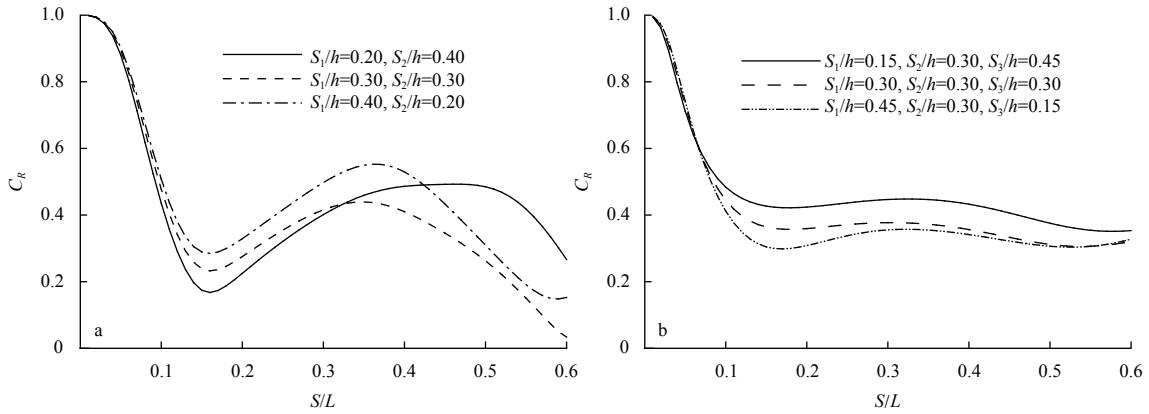

Fig. 9. Effect of the dimensionless chamber width S_j/h on the reflection coefficient C_R. a. Two-chamber perforated caisson breakwater and b. three-chamber perforated caisson breakwater.

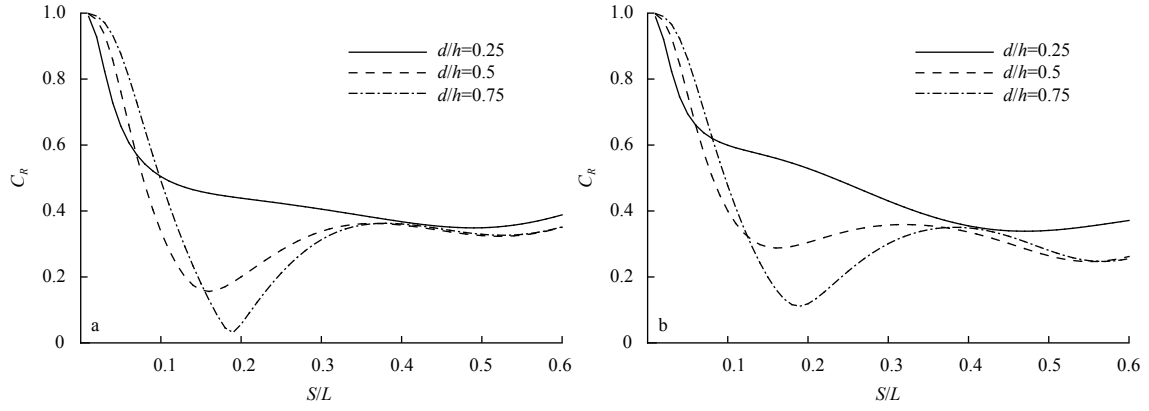

Fig. 10. Effect of the relative water depth in the chamber d/h on the reflection coefficient C_R. a. Two-chamber perforated caisson breakwater and b. Three-chamber perforated caisson breakwater.

drop condition on perforated walls, we have developed a fully iterative analytical solution for wave reflection by a multi-chamber partially perforated caisson breakwater. We have shown that the convergences of the present series solution and the iterative calculations were fast. We have also shown that the predictions by the present analytical solution were in excellent agreement with that by the multi-domain BEM solution. In addition, we have validated the present analytical solution using experimental data in literature.

We have presented calculation examples to clarify the hydrodynamic performance of multi-chamber partially perforated breakwaters. Compared to the single-chamber perforated caisson breakwater, the multi-chamber perforated caisson breakwater can have a better wave energy dissipation performance over a broad range of wave frequency, and may perform better if the perforated walls have a larger porosity. The perforated front walls should be designed with deceasing porosities along the incident wave propagation direction, which is helpful for dissipating more

incident wave energy. Using non-uniform wave chambers instead of uniform chambers may further decrease the reflection coefficient of the breakwater. But, the arrangement of non-uniform chambers needs to be carefully designed according to different chamber numbers.

The beauty of the present iterative solution is that the effect of wave height on the wave energy dissipation due to perforated walls can be well considered by the solution itself. The present solution is simple and reliable for fast assessing the hydrodynamic performance of perforated caisson breakwaters in preliminary engineering design. But, it should be noted that for practical application, the flow process across the perforated walls cannot be well considered by the present potential solution. Alternatively, a simple pressure drop condition has been used to describe the energy dissipation by the perforated walls. In addition, the effects of wave nonlinearity and possible wave breaking on wave scattering cannot be considered by the present linear solution. Moreover, the present solution only consider regular waves and it can be extended to irregular waves using the transfer function method (Liu et al., 2008a; Liu and Li, 2017).

References

Aristodemo F, Meringolo D D, Groenenboom P, et al. 2015. Assessment of dynamic pressures at vertical and perforated breakwaters through diffusive SPH schemes. Mathematical Problems in Engineering, 2015: 305028

Bennett G S, McIver P, Smallman J V. 1992. A mathematical model of a slotted wavescreen breakwater. Coastal Engineering, 18(3–4): 231–249

Bergmann H, Oumeraci H. 2000. Wave loads on perforated caisson breakwaters. In: Proceedings of the 27th International Conference on Coastal Engineering. Sydney, Australia: ASCE, 1622–1635

Chen Xuefeng, Li Yucheng, Sun Dapeng. 2002. Regular waves acting on double-layered perforated caissons. In: Proceedings of the Twelfth International Offshore and Polar Engineering Conference. Kitakyushu, Japan: International Society of Offshore and Polar Engineers, 736–743

Chen Xuefeng, Li Yucheng, Wang Yongxue, et al. 2003. Numerical simulation of wave interaction with perforated caisson breakwaters. China Ocean Engineering, 17(1): 33–43

Franco L. 1994. Vertical breakwaters: the Italian experience. Coastal Engineering, 22(1–2): 31–55

Franco L, De Gerloni M, Passoni G, et al. 1998. Wave forces on solid and perforated caisson breakwaters: comparison of field and laboratory measurements. In: Proceedings of the 26th International Conference on Coastal Engineering. Copenhagen, Denmark: ASCE, 1945–1958

Huang Zhenhua, Li Yucheng, Liu Yong. 2011. Hydraulic performance and wave loadings of perforated/slotted coastal structures: a review. Ocean Engineering, 38(10): 1031–1053, doi: 10.1016/j.oceaneng.2011.03.002

Isaacson M, Baldwin J, Premasiri S, et al. 1999. Wave interactions with double slotted barriers. Applied Ocean Research, 21(2): 81–91, doi: 10.1016/S0141-1187(98)00039-X

Jarlan G E. 1961. A perforated vertical wall breakwater. The Dock and Harbour Authority XII, (486): 394–398

Kakuno S, Liu P L F. 1993. Scattering of water waves by vertical cylinders. Journal of Waterway, Port, Coastal, and Ocean Engineering, 119(3): 302–322, doi: 10.1061/(ASCE)0733-950X(1993)119:3(302)

Kakuno S, Nakata Y. 1998. Scattering of water waves by rows of cylinders with/without a backwall. Applied Ocean Research, 20(4): 191–198, doi: 10.1016/S0141-1187(97)00026-6

Kakuno S, Shiozaki Y, Harayama Y. 1999. The effect of the depth of wave chambers of a double slit-wall breakwater on wave reflection. Proceedings of Civil Engineering in the Ocean (in Japanese), 15: 671–676, doi: 10.2208/prooe.15.671

Kondo H. 1979. Analysis of breakwaters having two porous walls. In: Proceedings of Coastal Structures '79. Alexandria: ASCE, 962–977

Koraim A S, Heikal E M, Rageh O S. 2011. Hydrodynamic characteristics of double permeable breakwater under regular waves. Marine Structures, 24(4): 503–527, doi: 10.1016/j.marstruc.2011.06.004

Lee J I, Kim Y T, Shin S. 2014. Experimental studies on wave interactions of partially perforated wall under obliquely incident waves. The Scientific World Journal, 2014: 954174

Li Yucheng, Dong Guohai, Liu Hongjie, et al. 2003. The reflection of oblique incident waves by breakwaters with double-layered perforated wall. Coastal Engineering, 50(1–2): 47–60

Li Yucheng, Liu Hongjie, Dong Guohai. 2005. The force of oblique incident wave on the breakwater with a partially perforated wall. Acta Oceanologica Sinica, 24(4): 121–130

Liu Yong, Li Huajun. 2017. Iterative multi-domain BEM solution for water wave reflection by perforated caisson breakwaters. Engineering Analysis with Boundary Elements, 77: 70–80, doi: 10.1016/j.enganabound.2016.12.011

Liu Yong, Li Yucheng, Teng Bin, et al. 2008a. Total horizontal and vertical forces of irregular waves on partially perforated caisson breakwaters. Coastal Engineering, 55(6): 537–552, doi: 10.1016/j.coastaleng.2008.02.005

Liu Yong, Li Yucheng, Teng Bin, et al. 2008b. Wave motion over a submerged breakwater with an upper horizontal porous plate and a lower horizontal solid plate. Ocean Engineering, 35(16): 1588–1596, doi: 10.1016/j.oceaneng.2008.08.003

Liu Yong, Li Yucheng, Teng Bin. 2012. Interaction between obliquely incident waves and an infinite array of multi-chamber perforated caissons. Journal of Engineering Mathematics, 74(1): 1–18, doi: 10.1007/s10665-011-9484-2

Liu Hongjie, Liu Yong, Li Yucheng. 2009. The theoretical study on diagonal wave interaction with perforated-wall breakwater with rock fill. Acta Oceanologica Sinica, 28(6): 103–110

Mei C C, Liu P L F, Ippen A T. 1974. Quadratic loss and scattering of long waves. Journal of the Waterways, Harbors and Coastal Engineering Division, 100(3): 217–239

Molin B, Fourest J M. 1992. Numerical modeling of progressive wave absorbers. In: Proceedings of the 7th International Workshop on Water Waves & Floating Bodies. Val de Reuil, France

Molin B. 2011. Hydrodynamic modeling of perforated structures. Applied Ocean Research, 33(1): 1–11, doi: 10.1016/j.apor.2010.11.003

Molin B, Remy F. 2015. Inertia effects in TLD sloshing with perforated screens. Journal of Fluids and Structures, 59: 165–177, doi: 10.1016/j.jfluidstructs.2015.09.004

Ren Xiaozhong, Ma Yuxiang. 2015. Numerical simulations for nonlinear waves interaction with multiple perforated quasi-ellipse caissons. Mathematical Problems in Engineering, 2015: 895673

Sollitt C K, Cross R H. 1972. Wave transmission through permeable breakwaters. In: Proceedings of the 13th International Conference on Coastal Engineering. Vancouver: ASCE, 1827–1846

Suh K D, Choi J C, Kim B H, et al. 2001. Reflection of irregular waves from perforated-wall caisson breakwaters. Coastal Engineering, 44(2): 141–151, doi: 10.1016/S0378-3839(01)00028-X

Suh K D, Ji C H, Kim B H. 2011. Closed-form solutions for wave reflection and transmission by vertical slotted barrier. Coastal Engineering, 58(12): 1089–1096, doi: 10.1016/j.coastaleng.2011.06.001

Suh K D, Park J K, Park W S. 2006. Wave reflection from partially perforated-wall caisson breakwater. Ocean Engineering, 33(2): 264–280, doi: 10.1016/j.oceaneng.2004.11.015

Taylor P J. 1973. The blockage coefficient for flow about an arbitrary body immersed in a channel. Journal of Ship Research, 17(2): 97–105

Yu Xiping. 1995. Diffraction of water waves by porous breakwaters. Journal of Waterway, Port, Coastal, and Ocean Engineering, 121(6): 275–282, doi: 10.1061/(ASCE)0733-950X(1995)121:6(275)

Zhao Yang, Liu Yong, Li Huajun, et al. 2017. Oblique wave motion over multiple submerged porous bars near a vertical wall. Journal of Ocean University of China, 16(4): 568–574, doi: 10.1007/s11802-017-3333-5

Appendix: Matrix coefficients in Eqs (30)–(33)

The matrix coefficients in Eqs (30)–(33) are listed in as follows:

$$c_{j,mn} = \sin\left(\lambda_0 \frac{S_j}{2}\right),\ m = n = 0, \tag{A1}$$

$$c_{j,mn} = \tanh\left(\lambda_m \frac{S_j}{2}\right),\ m = n \neq 0, \tag{A2}$$

$$c_{j,mn} = 0,\ m \neq n, \tag{A3}$$

$$d_{j,mn} = -\cos\left(\lambda_0 \frac{S_j}{2}\right),\ m = n = 0, \tag{A4}$$

$$d_{j,mn} = 1,\ m = n \neq 0, \tag{A5}$$

$$d_{j,mn} = 0,\ m \neq n, \tag{A6}$$

$$e_{j,mn} = \sin\left(\lambda_0 \frac{S_{j+1}}{2}\right),\ m = n = 0, \tag{A7}$$

$$e_{j,mn} = \tanh\left(\lambda_m \frac{S_{j+1}}{2}\right),\ m = n \neq 0, \tag{A8}$$

$$e_{j,mn} = 0,\ m \neq n, \tag{A9}$$

$$f_{j,mn} = \cos\left(\lambda_0 \frac{S_{j+1}}{2}\right),\ m = n = 0, \tag{A10}$$

$$f_{j,mn} = -1,\ m = n \neq 0, \tag{A11}$$

$$f_{j,mn} = 0,\ m \neq n, \tag{A12}$$

$$g_{mn} = \frac{\int_{-d}^{0} Z_n(z) Y_m(z)\,\mathrm{d}z}{\int_{-d}^{0} Y_m^2(z)\,\mathrm{d}z}, \tag{A13}$$

$$h_{mn} = -\lambda_0 \sin\left(\lambda_0 \frac{S_1}{2}\right) \frac{\int_{-d}^{0} \phi_1(z)\, Y_0(z)\, Y_m(z)\,\mathrm{d}z}{\int_{-d}^{0} Y_m^2(z)\,\mathrm{d}z} + \xi_{1,mn},\ n = 0, \tag{A14}$$

$$h_{mn} = \lambda_n \tanh\left(\lambda_n \frac{S_1}{2}\right) \frac{\int_{-d}^{0} \phi_1(z)\, Y_n(z)\, Y_m(z)\,\mathrm{d}z}{\int_{-d}^{0} Y_m^2(z)\,\mathrm{d}z} + \xi_{1,mn},\ n \neq 0, \tag{A15}$$

$$t_{mn} = -\lambda_0 \cos\left(\lambda_0 \frac{S_1}{2}\right) \frac{\int_{-d}^{0} \phi_1(z)\, Y_0(z)\, Y_m(z)\,\mathrm{d}z}{\int_{-d}^{0} Y_m^2(z)\,\mathrm{d}z} + \zeta_{1,mn},\ n = 0, \tag{A16}$$

$$t_{mn} = -\lambda_n \frac{\int_{-d}^{0} \phi_1(z)\, Y_n(z)\, Y_m(z)\, \mathrm{d}z}{\int_{-d}^{0} Y_m^2(z)\, \mathrm{d}z} + \zeta_{1,mn},\ n \neq 0, \tag{A17}$$

$$\sigma_m = -\frac{\int_{-d}^{0} Z_0(z) Y_m(z)\, \mathrm{d}z}{\int_{-d}^{0} Y_m^2(z)\, \mathrm{d}z}, \tag{A18}$$

$$p_{j,mn} = \cos\left(\lambda_0 \frac{S_j}{2}\right),\ m = n = 0, \tag{A19}$$

$$p_{j,mn} = 1,\ m = n \neq 0, \tag{A20}$$

$$p_{j,mn} = 0,\ m \neq n, \tag{A21}$$

$$q_{j,mn} = \sin\left(\lambda_0 \frac{S_j}{2}\right),\ m = n = 0, \tag{A22}$$

$$q_{j,mn} = \tanh\left(\lambda_m \frac{S_j}{2}\right),\ m = n \neq 0, \tag{A23}$$

$$q_{j,mn} = 0,\ m \neq n, \tag{A24}$$

$$r_{j,mn} = -\lambda_0 \sin\left(\lambda_0 \frac{S_{j+1}}{2}\right) \frac{\int_{-d}^{0} \phi_{j+1}(z)\, Y_0(z)\, Y_m(z)\, \mathrm{d}z}{\int_{-d}^{0} Y_m^2(z)\, \mathrm{d}z} + \xi_{j+1,mn},\ n = 0, \tag{A25}$$

$$r_{j,mn} = \lambda_n \tanh\left(\lambda_n \frac{S_{j+1}}{2}\right) \frac{\int_{-d}^{0} \phi_{j+1}(z)\, Y_n(z)\, Y_m(z)\, \mathrm{d}z}{\int_{-d}^{0} Y_m^2(z)\, \mathrm{d}z} + \xi_{j+1,mn},\ n \neq 0, \tag{A26}$$

$$s_{j,mn} = -\lambda_0 \cos\left(\lambda_0 \frac{S_{j+1}}{2}\right) \frac{\int_{-d}^{0} \phi_{j+1}(z)\, Y_0(z)\, Y_m(z)\, \mathrm{d}z}{\int_{-d}^{0} Y_m^2(z)\, \mathrm{d}z} + \zeta_{j+1,mn},\ n = 0, \tag{A27}$$

$$s_{j,mn} = -\lambda_n \frac{\int_{-d}^{0} \phi_{j+1}(z)\, Y_n(z)\, Y_m(z)\, \mathrm{d}z}{\int_{-d}^{0} Y_m^2(z)\, \mathrm{d}z} + \zeta_{j+1,mn},\ n \neq 0, \tag{A28}$$

$$u_{mn} = \sin\left(\lambda_0 \frac{S_N}{2}\right),\ m = n = 0, \tag{A29}$$

$$u_{mn} = \tanh\left(\lambda_m \frac{S_N}{2}\right),\ m = n \neq 0, \tag{A30}$$

$$u_{mn} = 0,\ m \neq n, \tag{A31}$$

$$v_{mn} = -\cos\left(\lambda_0 \frac{S_N}{2}\right),\ m = n = 0, \tag{A32}$$

$$v_{mn} = 1,\ m = n \neq 0, \tag{A33}$$

$$v_{mn} = 0, m \neq n, \tag{A34}$$

$$\xi_{j,mn} = -\cos\left(\lambda_0 \frac{S_j}{2}\right) + 2C_j\lambda_0 \sin\left(\lambda_0 \frac{S_j}{2}\right),\ m = n = 0, \tag{A35}$$

$$\xi_{j,mn} = -1 - 2C_j\lambda_m \tanh\left(\lambda_m \frac{S_j}{2}\right),\ m = n \neq 0, \tag{A36}$$

$$\xi_{j,mn} = 0,\ m \neq n, \tag{A37}$$

$$\zeta_{j,mn} = \sin\left(\lambda_0 \frac{S_j}{2}\right) + 2C_j\lambda_0 \cos\left(\lambda_0 \frac{S_j}{2}\right),\ m = n = 0, \tag{A38}$$

$$\zeta_{j,mn} = \tanh\left(\lambda_m \frac{S_j}{2}\right) + 2C_j\lambda_m,\ m = n \neq 0, \tag{A39}$$

$$\zeta_{j,mn} = 0,\ m \neq n, \tag{A40}$$

$$\phi_j(z) = \frac{2\mathrm{i}gH}{3\pi\omega^2}\frac{1-\varepsilon_j}{\mu_j\varepsilon_j^2}\begin{vmatrix} A_{j,0}\lambda_0 \sin\left(\lambda_0\frac{S_j}{2}\right) Y_0(z) - \sum_{n=1}^{\infty} A_{1,n}\lambda_n \tanh\left(\lambda_n \frac{S_j}{2}\right) Y_n(z) + \\ B_{j,0}\lambda_0 \cos\left(\lambda_0\frac{S_j}{2}\right) Y_0(z) + \sum_{n=1}^{\infty} B_{j,n}\lambda_n Y_n(z) \end{vmatrix}. \tag{A41}$$